Real-Time Kinetic Measurements of the Condensation and Evaporation of D_2O Molecules on Ice at 140 K < *T* < 220 K

Laurent Chaix, Hubert van den Bergh, and Michel J. Rossi*

Laboratoire de Pollution Atmosphérique et Sol (LPAS), Environmental Engineering Institute (DGR/IGE), Ecole Polytechnique Fédérale de Lausanne (EPFL), CH-1015 Lausanne/Switzerland

Received: July 16, 1998; In Final Form: September 14, 1998

The kinetics of condensation of $D_2{}^{18}O$ water vapor on $D_2{}^{16}O$ ice was studied in the temperature range 140−220 K. The measurements have been performed in real time using the pulsed valve technique in a low-pressure flow reactor. Ice samples were prepared by several different methods. The uptake coefficient γ was observed to decrease with increasing surface temperature, and varied from $\gamma = 0.06$ to 0.8. A significant dependence of γ on the method of preparation of the ice has been found. At 180 K, $\gamma = 0.13$ for single-crystal ice, 0.18 for ice condensed from the vapor phase, and approximately 0.25 for bulk ice obtained from freezing liquid $D_2{}^{16}O$. The uptake coefficient attained a value of $\gamma = 0.8$ at 140 K for cubic ice prepared by vapor condensation at 140 K. The activation energy for evaporation of D_2O at low temperatures (140−190 K) has been measured as 12.2 kcal/mol, whereas it decreases to 8.3 kcal/mol at higher temperatures (190−220 K). The rate of evaporation at 200 K corresponds to the loss of approximately 70 ± 10 formal monolayers per second. The experimental results suggest the formation of loosely bound water adsorbed to the surface of ice whose bond energy is estimated to be 4.0 ± 0.4 kcal/mol, independent of the type of ice.

Introduction

Ice nuclei exist in the earth's atmosphere both as free particulates and embedded in cloud particles and hydrometeors. Therefore, tropospheric and stratospheric clouds often contain ice.[1,2] Moreover, ice is also an important constituent of atmospheric aerosols.[1] Ice particles may originate in clouds by deposition from the vapor phase or by the nucleation of supercooled water droplets.[3−5] In short, condensation and evaporation of water on ice is essential to the occurrence and formation of ice particles in the atmosphere, as well as to cloud formation and growth.[6] Consequently, condensation and evaporation of water vapor on ice are among the most important fundamental atmospheric processes because thet control the generation and growth of natural ice particles, which are thought to be important in global climate change issues.

The measurement of the condensation coefficient of H_2O on ice is therefore expected to be important in models describing the growth kinetics of polar stratospheric clouds (PSCs), for the prediction of PSCs lifetimes and size distributions in the stratosphere, and for cloud physics[7] in general. Ice also plays an important role in the chemistry of aircraft contrails[8] in the upper atmosphere, especially at high cruising altitude (from 8 to 13 km). In addition, the rate of cirrus cloud growth seeded by natural or contrail particles formed in jet aircraft exhaust plumes is an active field of investigation in need of fundamental kinetic parameters. Thus, a detailed knowledge of the condensation and evaporation coefficient of H_2O on ice seems to be important for modeling multiple heterogeneous processes in the lower stratosphere as well as in the upper stratosphere.

Measurements of the uptake coefficient of water on ice have been the subject of numerous experimental investigations using various techniques, such as gravimetric methods,[9,10] and molecular beam and optical interference techniques.[11,12] These methods were aimed at investigating the changes on the ice surface, whereas other techniques are based on the measurement of the vapor phase in a closed system or in a fast-flow reactor.[13,14] Experimental values of the uptake coefficients range from approximately $\gamma = 0.03$ to unity,[11] depending on the surface temperature, on the experimental technique, or on the type of ice used. Actually, no study has succeeded in establishing the cause of this variability in the value of γ. In addition, a number of previous experiments have been performed at temperatures where evaporation could not be neglected. Therefore, in such experiments, the rate of evaporation could not be separated from condensation.[15,16] To separate both processes, the hypothesis was made in most of these studies that the condensation and evaporation coefficients were identical.[15,17] However, this assumption has been shown to be inappropriate.[18] The present experimental results, together with a proposed simple mechanism, contribute toward a fundamental understanding of the detailed processes of H_2O condensation and evaporation on ice at low temperatures. At the end of this paper, we will discuss some of the implications of this work for the growth and dynamic equilibrium of ice particles in the atmosphere, as well as for some aspects of atmospheric chemistry.

Experimental

We describe the real-time kinetic measurement of the condensation rate constants and the rate of evaporation of water vapor on ice. These kinetic studies have been performed using a low-pressure flow reactor. To experimentally separate the evaporation rate of the ice matrix from the condensation rate of the probe molecules, the ice samples have been prepared from $D_2{}^{16}O$, monitored at $m/e = 20$, whereas the condensing water injected into the reactor consisted of $D_2{}^{18}O$, monitored at $m/e = 22$. Therefore, the term "ice" used in this paper represents the condensed phase and always refers to $D_2{}^{16}O$. The

* To whom correspondence should be addressed.

10.1021/jp983050n CCC: $15.00
Published on Web 11/17/1998

TABLE 1: Characteristic Parameters of the Knudsen Cell Used in This Study

definition	symbol	expression	numerical value[a]
volume	V		1830 cm^3
estimated reactor surface area	A_H		1300 cm^2
diameter of escape orificice	D_0		4, 8, 14 mm
escape rate constant at $D_0 = 14$ mm	k_{esc}[b]	$k_{esc} = 1.77(T/M)^{0.5}$	$k_{esc} = 6.64\ s^{-1}$
gas number density	N	$N = F_i/(Vk_{esc})$[c]	$(1-100) \times 10^9\ cm^{-3}$
sample surface area[d]	A_s		$A_s^1 = 15.9\ cm^2$
			$A_s^2 = 8\ cm^2$
collision frequency on surface[d]	ω	$\omega = A_s(T/M)^{0.5}$	$\omega^1 = 132\ s^{-1}$
			$\omega^2 = 66.4\ s^{-1}$
uptake coefficient	γ	$\gamma = k_{eff}/\omega$	

[a] Calculated using the mass of the $D_2{}^{16}O$ molecule (22 amu). [b] Values determined directly by experiment. [c] F_i is the flow of molecules per second. [d] Superscripts 1 and 2 refer to two cryogenic sample holders of different geometry.

rate of condensation and evaporation of $D_2{}^{18}O$ molecules at ambient temperatures on a $D_2{}^{16}O$ ice surface has been measured at substrate temperatures ranging from 140 to 220 K. These results have been interpreted using a mechanism made up of elementary gas and surface processes, leading to the incorporation of $D_2{}^{18}O$ into bulk ice. The present measurements demonstrate the influence of the method of ice preparation or of its thermal history on the measured kinetic parameters.

The experiments have been performed using a Teflon-coated Knudsen reactor, which was part of a flowing gas experiment. A detailed account of this technique has been given elsewhere.[19,20] Briefly, the Knudsen reactor is mounted on a vacuum chamber fitted with a quadrupole mass spectrometer. A given number of gas molecules are injected into the reactor, using a pulsed valve, after which they effuse out of the escape orifice. During their lifetime τ in the gas phase, which is the inverse of the measured effusion rate constant k_{esc}, the molecules undergo several thousand collisions with the coated wall and interact with the surface of interest. An effusing molecular beam is formed at the escape orifice and is monitored as a function of time using phase-sensitive mass spectrometric detection after it has been modulated using a rotating chopper wheel. The loss of the vapor phase onto the ice is in competition with the loss through the escape aperture and is compared to reference experiments in which the ice sample is isolated from the interacting flow. Absolute concentrations of water vapor in the flow reactor are derived from calibration of the MS signals with absolute flow rates obtained by recording the pressure change in a calibrated volume as a function of time.

We have performed two types of experiments: continuous flow and pulsed valve experiments.[20] Most of the reported experiments correspond to transient supersaturation using a pulsed valve through which short pulses of several milliseconds in duration of water vapor were introduced into the reactor. The molecules effusing out of the Knudsen cell have been monitored in real time by mass spectrometry. In reactive experiments, in which the ice sample has been exposed to a $D_2{}^{18}O$ burst, the signal decay (k_{dec}) is due to two independent competing processes, namely the measured rate of escape (k_{esc}) and the condensation rate (k_{eff}).

$$S(t) = S_0 \exp(-(k_{esc} + k_{eff})t) \tag{1}$$

By fitting the decay of both a reference pulse (k_{esc}) taken in the absence of the ice sample and a reactive pulse ($k_{dec} = k_{esc} + k_{eff}$) we obtain k_{eff} for the condensation of $D_2{}^{18}O$ molecules on ice (Table 1). Under molecular flow conditions, we calculate the collision frequency ω of the average molecule with the sample according to eq 2,

$$\omega = (\langle c \rangle / 4V) A_s \tag{2}$$

where $\langle c \rangle$ is the average molecular velocity of the gas, A_s the geometric surface of the ice sample, and V is the volume of the cell. The uptake coefficient γ is then determined from the measured rate constant k_{eff} according to eqs 3 and 4.

$$d\frac{[D_2O]}{dt} = -k_{eff}[D_2O] \tag{3}$$

The measurement of k_{eff}, thus of γ, is based on the net change

$$\gamma = k_{eff}/\omega \tag{4}$$

of the water partial pressure with time in the presence of an ice substrate. It therefore takes into account the rate of evaporation of ice. If the evaporation rate is insignificant compared to condensation, that is at low temperature, the net uptake coefficient will be equal to the condensation coefficient, which has often been called the sticking coefficient in the past.

Most experiments have been performed using the 14 mm escape aperture in order to study fast uptake rates. The signal was recorded using the MS/lock-in detection combination at $m/e = 22$ for $D_2{}^{18}O$. Because of the fast decay rates of the reactive pulse, a sampling frequency of 500 Hz was needed.

We avoid surface saturation owing to large doses of $D_2{}^{18}O$ by using the pulsed valve technique. The doses were determined from the integral of the MS signal $S(t)$ of the corresponding reference pulses. The amount injected was varied by changing the opening period of the solenoid valve or the $D_2{}^{18}O$ backing pressure in the gas supply line. Typical $D_2{}^{18}O$ doses were in the range $10^{15}-10^{18}$ molecules per pulse, corresponding to the condensation of approximately 10% up to several formal monolayers of condensed $D_2{}^{18}O$ molecules.

To attain the present temperature range (140−220 K), we used a sample holder described elsewhere.[21] To test whether the sample preparation procedure had a significant impact on the uptake kinetics, five different types of ice samples have been prepared. The first, referred to as the bulk sample (B), consists of liquid $D_2{}^{16}O$ water that has been poured into the well of the sample holder at ambient temperature and rapidly frozen down to 160 K within approximately 4 min. This sample was subsequently annealed at 240 K during 20 min. To avoid the inclusion of air bubbles in the crystal, the $D_2{}^{16}O$ was previously degassed by freeze−pump−thaw cycles in a vacuum line. The second, referred to as single-crystal ice (SC), has been obtained by freezing deionized $D_2{}^{16}O$ water at a very slow rate in order to avoid the buildup of stress during crystal growth. The cooling rate was approximately 1/3 K/min. We assume that this type of ice sample is characterized by very low surface defect densities such as dislocations or cracks.[1]

The other samples have been obtained by condensation of $D_2{}^{16}O$ from the vapor phase by admitting a $D_2{}^{16}O$ flow onto

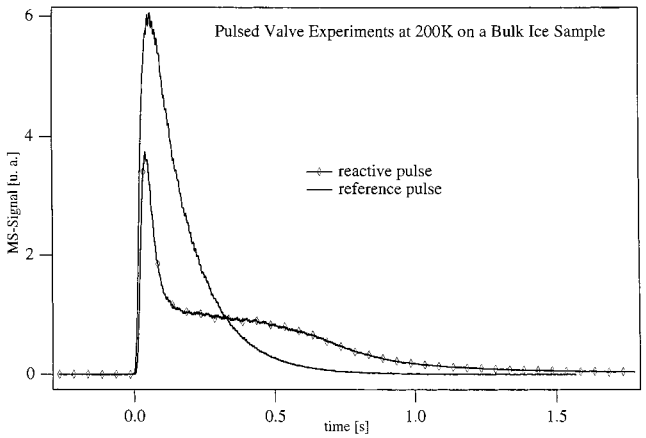

Figure 1. Typical pulsed valve experiments of $D_2{}^{18}O$ vapor on a bulk ice sample of $D_2{}^{16}O$ at 200 K. The reference pulse corresponds to the decay of the MS signal at $m/e = 22$ in real time in the absence of ice where the reactive pulse corresponds to the presence of ice.

the sample well at the temperature of interest. Exposure of this flow to the cold copper substrate of the sample well for a given time resulted in a thick ice film equivalent to a few thousand monolayers depending on the dose. The texture of the deposit is porous, depending on the choice of the temperature of formation.[22] Two types of ice condensed at 180 K from the vapor phase have been investigated, namely C_1 and C_2 depending on the $D_2{}^{16}O$ flow rate, which was adjusted typically between 10^{16} molecules s^{-1} (C_1) and 10^{14} molecules s^{-1} (C_2), respectively.

Following the literature,[22, 23] we assume that the structure of films deposited at 140 K from the vapor phase is cubic (K), although there is still a large uncertainty in the accurate temperature of phase transition between amorphous and cubic ices. The ice we call cubic may in fact consist of a mixture of amorphous and cubic ices. At temperatures higher than 180 K, the condensed ice samples are polycrystalline in nature and consist of a mixture of cubic and hexagonal ice.[24] In addition, for ices condensed at 180 K, the degree of crystallinity is known to depend on the deposition rate.[25] Because the growth rates in the atmosphere are slowest for natural snow crystals, ice grown at slow rates from the vapor phase has garnered increased attention during the present work. Thus, we have prepared ice samples by vapor condensation on the cold sample holder (200 K) at ambient pressure. At 1 atm, the growth rate of ice is limited by molecular diffusion of $D_2{}^{16}O$ toward the crystal surface.[26,27] This type of ice had the appearance of a fluffy powder and is referred to as "snow" (S) in this work, because it resembles powdery snow inasmuch as appearance is concerned. During the kinetic measurements, all the ice samples were kept at equilibrium under steady-state conditions by setting an additional constant external $D_2{}^{16}O$ flow so as to cancel evaporation and condensation rates, thus resulting in no net water vapor uptake.

Results

A typical result of a transient supersaturation experiment is shown in Figure 1. In this example, the pulsed valve was opened at 0.2 s for 1 ms resulting in a dose of 5×10^{15} molecules injected into the Knudsen cell corresponding to approximately 0.5 nominal monolayers. The $D_2{}^{18}O$ molecules interact with ice and the resulting MS signal was monitored as a function of time. Typically, the pulses depend on the dose, the temperature, and the type of ice sample used. A reference pulse in the absence of an ice substrate is characterized by a single-exponential decay k_{dec} and simply corresponds to the effusion of $D_2{}^{18}O$. The second

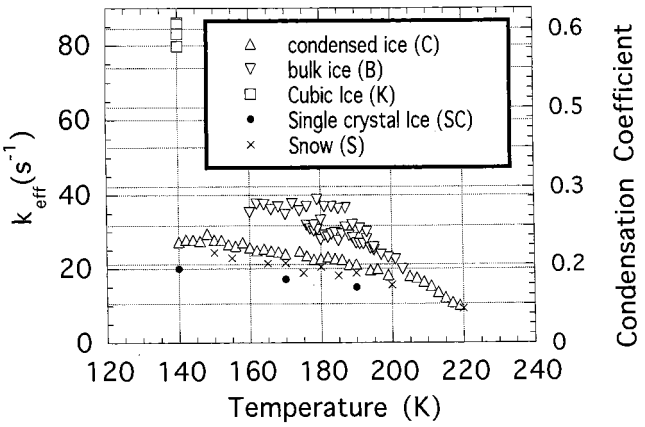

Figure 2. Temperature dependence of k_{eff} measured in pulsed valve experiments for five different types of ice samples. A typical dose of 5×10^{16} $D_2{}^{18}O$ molecules was used throughout.

TABLE 2: Typical Sample Data k_{eff} versus Temperature for Five Different Types of Ice

	temperature (K)								
ice[a]	140	150	160	170	180	190	200	210	220
SC	18.6			17		15.1			
	20	19.1	17	16	17.2	18	15		
B			35.3	34.8	33.2				
					38.8	31	22.5		
				30.7	31.8	26.9	24		
				35.3	34.8	33.2	22.5		
C_1	38	34.4	35	32.2	32.1	33.3	29.2		
C_2				24.9	23.8	22.3	20	14.9	9.3
			23.8	24.7	23.5	21.9	20.1	14	
				24.9	24.7	21.9	20	14.9	9.6
	27.8	28.3	27.5	24.6	23.2	20.3	16.7	16.1	10
	27.3	27.8	25.7	24	22.7	21.1	18.3	15.4	10.2
K	74.7[b]								
	74.9[b]								
	81.4[b]								
S		23	23.2	20.2	20.0	19.5	14.5	9.2	

[a] Symbols are explained in the text. [b] Corrected according to ref 21 for the density gradient in the Knudsen cell. The correction factor equals approximately 1.2 (ref 21).

type is followed by the formation of a steady-state level after prior single-exponential decay. The signal remains constant for a few seconds and subsequently decreases to its initial background level. This steady-state level originates from the balance between the rate of condensation k_{cond} [$D_2{}^{18}O$], the rate of evaporation R_{ev}, and the escape of the molecules out of the reactor, k_{esc}[$D_2{}^{18}O$]. The height of this steady-state level depends on the temperature and thus is related to the $D_2{}^{18}O$ equilibrium vapor pressure.

We first measured the rate constant for condensation (k_{eff}) on various types of ice samples at temperatures ranging from 140−220 K. The dose of $D_2{}^{18}O$ used for all the uptake measurements is equivalent to 50% of a formal monolayer, corresponding to approximately 5×10^{15} molecules. The temperature range used in this study was given by the stability of the corresponding ice samples. The uptake coefficients are calculated from measured values of k_{eff} by dividing through the appropriate values of ω corresponding to experiments in several flow reactors of different sample areas A_s (Table 1).

The results for the five different types of ice substrates are displayed in Figure 2 and summarized in Table 2. We have tested the thermal stability of each ice sample during experimental runs by investigating potential hysteresis effects on k_{eff} by first increasing the sample temperature from 140 to 220K and then decreasing it, as shown in Figure 3. Since no hysteresis was detected, it may be concluded that the sample surface is

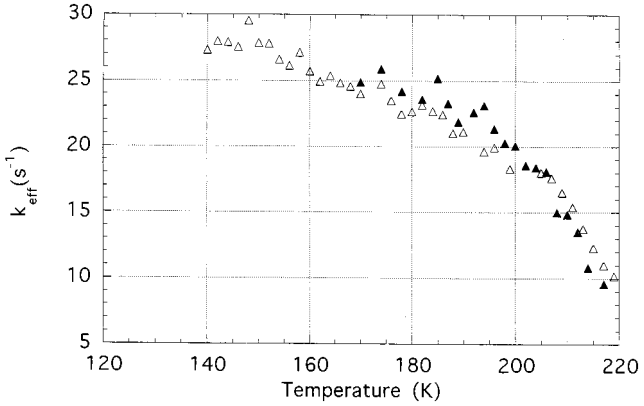

Figure 3. Temperature dependence of k_{eff} obtained in pulsed valve experiments on an ice sample (C) condensed at 170 K. The experiment was started at 170 K by increasing the temperature to 220 K (▲). Subsequently, the surface temperature was decreased from 220 to 140 K (△).

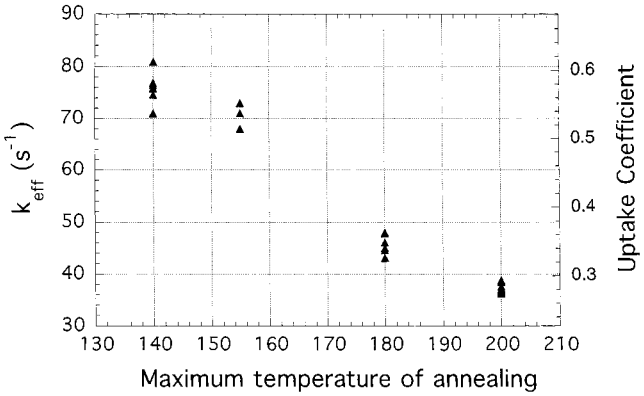

Figure 4. Effect of temperature on k_{eff} measured at 140 K. The cubic ice sample (K) was obtained by condensation of water vapor at 140 K. The displayed temperature is the maximum value to which the sample was annealed before performing the uptake measurement at 140 K.

stable during uptake measurements. A significant negative temperature dependence of k_{eff} is observed for four samples (Figure 2). The data show two distinct regimes of temperature dependence. In the low-temperature regime, a slight negative temperature dependence is observed. At higher temperatures, the dependence is more pronounced, and for all three ice samples investigated, γ drops to 0.06 when the sample temperature reaches 220 K. One of the main conclusions of this work is that the uptake coefficient of $D_2{}^{18}O$ on ice significantly varies between 0.06 and 0.8 in the temperature range 140−220 K.

The magnitude of the uptake coefficient seems to be strongly influenced by the type of ice sample (Figure 2). The present work deals with the kinetic consequences of different structural features of ice synthesized in the laboratory. We refrain from structural proof of the ice investigated and simply follow the published procedures in order to obtain ice of a certain type. At 140 K, we observe a value of $\gamma = 0.8$ on cubic ice (K), whereas $\gamma = 0.16$ has been measured on single-crystal ice (SC) at the same temperature. Because the values of k_{eff}, and hence of γ, seem to be very sensitive to the nature of the ice sample, we have measured k_{eff} at 140 K on four condensed cubic ice samples (K) after which they were annealed at different temperatures and subsequently cooled to 140 K for another measurement of k_{eff}. The results are shown in Figure 4; k_{eff} drops significantly when cubic ice (K) is annealed at 180 and 200 K, leading to a value identical to that for a bulk ice sample (B) measured at 140 K.

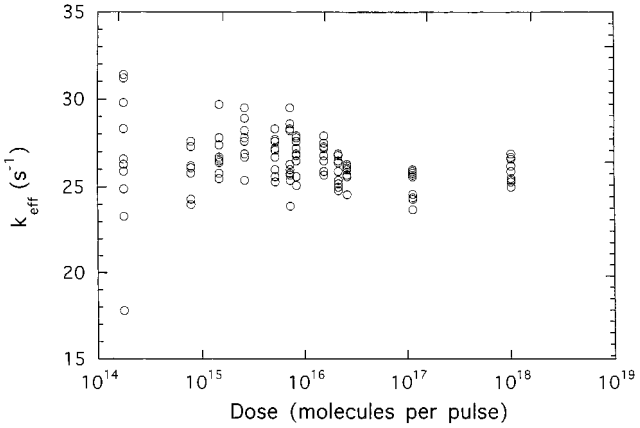

Figure 5. Dose dependence of k_{eff} measured in pulsed valve experiments at 195 K on a condensed ice (C) sample.

TABLE 3: Typical Mean Values of k_{eff} versus Temperature for Four Different Types of Ice (See Text for Explanation of Symbols)

type of ice samples	temperature (K)	$k_{eff\,(s-1)}$
C_2	175	26.4 ± 0.9
	180	25.3 ± 0.6
	195	16.9 ± 1.3
	190	15.8 ± 4
	140	28 ± 3
B	180	47.8 ± 6
	190	31.8 ± 4
	200	39.7 ± 3
SC	140	20 ± 4
K	140	75 ± 10

Additional experiments have been performed to investigate the dose dependence of the pulsed condensation process conducted as a transient supersaturation experiment. Results, displayed in Figure 5, have been obtained for a condensed ice sample (C) at 180 K. The injected dose was varied over 4 orders of magnitude. This range was obtained by changing the pulse length as well as the $D_2{}^{18}O$ backing pressure. The lower limit (approximately 10^{14} molecules per pulse) is given by the sensitivity limit of the mass spectrometer, whereas the high end of the dose range of approximately 10^{18} molecules per pulse is given by molecular flow limitations. As shown in Figure 5, no dose dependence is observable at 180 K within experimental error. Other experiments, summarized in Table 3, clearly indicate that no dose dependence is observed at other temperatures (160−210 K) either for all types of ice investigated. These results thus confirm the first-order rate law of k_{eff} for all types of ice in the temperature range 140−220K.

Finally, Figure 6 shows the vapor pressure as a function of reciprocal temperature calculated from k_{eff} and the steady-state part of the MS signal after pulsed condensation (Figure 1) for different types of ice samples. For doses exceeding a certain threshold value, the formation of a steady-state level is observed after the decay of the pulse (Figure 1). This level corresponds to the equilibrium vapor pressure of $D_2{}^{18}O$ at steady-state sustained by the rate of evaporation R_{ev}, which persists for a given amount of time depending on the quantity of $D_2{}^{18}O$ condensed on top of bulk $D_2{}^{16}O$. To calculate the equilibrium vapor pressure, we have used k_{eff} and determined the rate of evaporation, F_{ev}, from the steady-state level F_{ss}, which appears after the pulse. It is thus possible to separately determine k_{eff} and F_{ev} within the same pulsed valve experiment if a steady state is established on a particular ice sample such as on bulk ice (B). F_{ev} is calculated according to eq 5 based on a simple two-state equilibrium model for H_2O condensation and evapora-

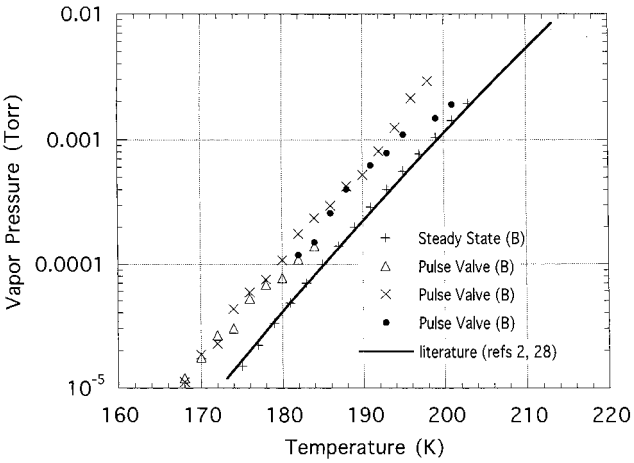

Figure 6. The calculated vapor pressure in the temperature range 170−200 K. The measurements have been performed on a bulk ice (B) sample, where the measurements (+) and (△) have been performed on the same sample. The solid line is the value of the equilibrium vapor pressure according to Jancso et al.[28]

SCHEME 1

$$H_2O_{(gas)} \underset{F_{ev}}{\overset{k_{cond}}{\rightleftharpoons}} H_2O_{(bulk)}$$

tion given in Scheme 1 where k_{cond} is set equal to the observed rate constant k_{eff}.

$$F_{ev} = F_{ss}\left(1 + \frac{k_{eff}}{k_{esc}}\right) \tag{5}$$

With kinetic data on condensation (k_{eff}) and evaporation (F_{ev}), the equilibrium vapor pressure P_{eq} of $D_2{}^{18}O$ may be calculated according to eq 6:

$$P_{eq} = \frac{R_{ev}}{k_{eff}}RT = \frac{F_{ev}}{k_{eff}V}RT \tag{6}$$

The calculated equilibrium vapor pressure P_{eq} displayed in Figure 6 for bulk ice samples on the basis of transient data (k_{eff}) is higher by a factor of 3 compared to literature values. For example, we have determined a value of 2×10^{-3} Torr at 200 K compared to 8×10^{-4} Torr given by Jancso et al. and Marti and Mauersberger.[2,28] However, steady-state evaporation experiments on bulk ice (B) using two different reactor orifices, which are not discussed in detail at this point but which are on display in Figure 6, lead to equilibrium vapor pressures in agreement with literature values. For the "snow" ice sample (S), no steady-state level has been observed, even for high doses of 10^{18} molecules per pulse, presumably due to fast surface diffusional processes of $D_2{}^{18}O$ into internal adsorption sites of snow in deeper layers of the sample.

Discussion

The pulsed valve technique provides a convenient method to measure the kinetics of heterogeneous processes in real time. To characterize the process of condensation and evaporation of water on ice and its mechanism, we have investigated the dependence of the kinetic constants on various parameters such as temperature, injected dose, or the manner in which the ice samples have been prepared.

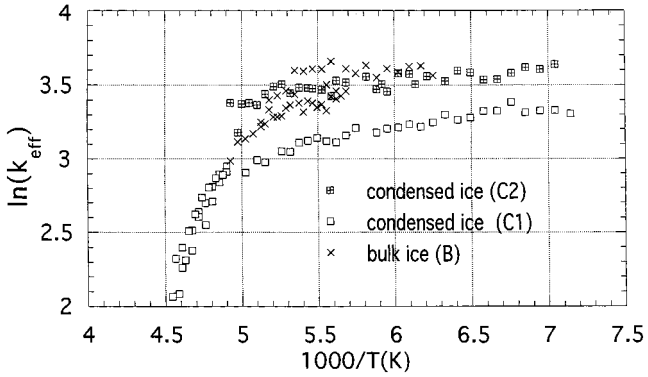

Figure 7. Arrhenius representation of the condensation rate constant k_{eff} obtained in pulsed valve experiments for three different ice samples. C_1 and C_2 refer to ice condensed from the vapor phase using high and low flow rates of $D_2{}^{18}O$, respectively.

TABLE 4: Activation Energies E_a of k_{eff} Measured in Two Different Temperature Ranges for Four Different Types of Ice

type of ice sample	E_a (kcal/mol)[a]	E_a (kcal/mol)[b]
B	-0.26 ± 0.13	-4.3 ± 1.7
C_2	-0.24 ± 0.05	-4.2 ± 1
C_1	-0.28 ± 0.07	
SC	-0.25 ± 0.08	

[a] Low-temperature range (140−190 K). [b] High-temperature range (190−220 K).

Temperature and Dose Dependence of k_{eff}: Standard Enthalpy of Sublimation ΔH_{sub} of Ice. As indicated in the previous section, all experiments performed on various types of ice reveal a pronounced negative dependence of k_{eff} on temperature. An Arrhenius representation is displayed in Figure 7. It clearly shows two distinct regimes of temperature dependence for each sample. In the high-temperature regime, k_{eff} changes faster with temperature compared to the low-temperature regime; γ drops to 0.06 for all types of ice at 220 K. Because these latter measurements have been performed at temperatures where the ice sublimation rate is appreciable, these low values of γ may be attributed to competitive evaporation resulting in a significant decrease of the net $D_2{}^{18}O$ uptake. The temperature of transition between these two regimes depends on the type of ice. The transition occurs at 200 K for a condensed ice sample (C_1,C_2) and at approximately 190 K for bulk ice (B).

From the temperature dependence of the kinetics, we have determined the activation energy of the condensation and evaporation process. Surprisingly, the values of the negative activation energies of k_{eff} seem to be independent of the type of ice. Table 4 displays some of the calculated values of the Arrhenius activation energy E_a. In the high-temperature regime, the mean energy of activation of k_{eff} is -4.3 ± 1.5 kcal/mol. The uptake data in the low-temperature regime lead to negative activation energies of -0.25 ± 0.08 kcal/mol. The values for the net rate of evaporation R_{ev} calculated according to eq 5 lead to a positive activation energy for evaporation E_{ev} of 8.3 ± 2 kcal/mol. The rate of evaporation F_{ev} reveals the surface to be very dynamic as has been pointed out before;[11] at 200 K about 70 ±10 monolayers s^{-1} of $D_2{}^{18}O$ evaporate and condense at equilibrium (Figure 8). By taking the difference of the activation energies of k_{eff} and F_{ev} calculated from steady-state levels in the corresponding range of temperature, we arrive at the heat of sublimation ΔH_{sub} of ice. As shown in Table 5, whatever the nature of the ice sample, the difference in activation energies

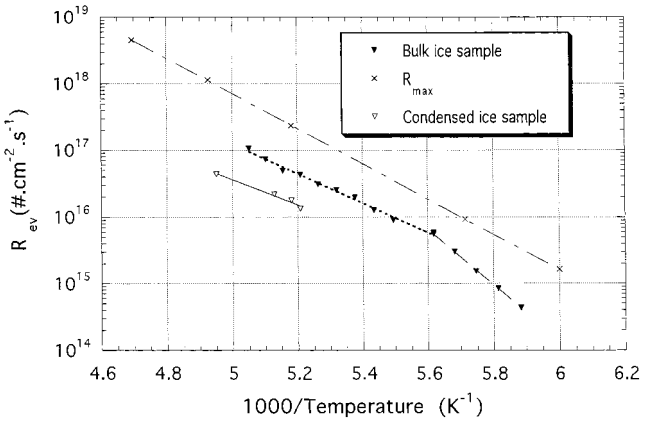

Figure 8. The rate of evaporation measured on bulk ice (B) samples in the temperature range 170−200K from pulsed valve experiments.

TABLE 5: Activation Energy of F_{Ev} and k_{eff} Measured in Two Different Temperature Ranges for Bulk Ice (B)

temperature range (K)	E_{cond} (kcal/mol)	E_{ev} (kcal/mol)
140−190K	-0.24 ± 0.1	$+12.2 \pm 0.5$
190−220K	-4.2 ± 1.7	$+8.3 \pm 1$

of k_{eff} and F_{ev} in the low-temperature regime results in a standard heat of sublimation $\Delta H_{sub} = 12.5 \pm 0.6$ kcal/mol. This value is in good agreement with the literature value of 12.2 kcal/mol[28] deduced from the measurement of the temperature dependence of the vapor pressure of H_2O over ice. At this point, we would like to underline the thermochemical relation of the condensation and evaporation processes where the difference of the measured activation energies $E_{cond} - E_{ev}$ closely matches the enthalpy of sublimation ΔH_{sub} as obtained from a separate experiment.

Water Vapor Pressure. To provide an independent check on the consistency between k_{eff} and R_{ev}, the equilibrium vapor pressure of water has been calculated as a function of temperature. The values of P_{eq} obtained when using k_{eff} from bulk (B) and single-crystal ice (SC) are higher by a factor of 3 or 4 and therefore in disagreement with literature data.[2,28] This apparent discrepancy may be attributed to the way the experiment has been performed, namely as a transient supersaturation experiment of $D_2{}^{18}O$ in the presence of $D_2{}^{16}O$ ice. An increase in the transient vapor pressure of $D_2{}^{18}O$ of a factor of 3 or so in the range 170−220 K is equivalent to warming the ice surface by 5 K. However, we attribute this transient increase in $D_2{}^{18}O$ over ice to the presence of a loosely bound precursor species in the aftermath of pulsed condensation for two reasons: (a) the extent of the increase of the $D_2{}^{18}O$ vapor pressure is independent of the dose of $D_2{}^{18}O$ used to perform the experiment and (b) steady-state uptake experiments, for which a larger warming of the ice surface is expected, fail to show any discrepancy with the equilibrium measurements of Jancso et al.[28] and Marti and Mauersberger.[2] The kinetic model involving the precursor will be discussed below. Figure 9 shows that the condensation of $D_2{}^{18}O$ molecules detected at $m/e = 22$ practically covers up the $D_2{}^{16}O$ ice surface and for a short time prevents to a large degree the evaporation of $D_2{}^{16}O$ detected at $m/e = 20$ (lower trace in Figure 9). The resulting perturbed total water vapor pressure is therefore made up of contributions of $D_2{}^{16}O$ and $D_2{}^{18}O$ as may be seen from a superposition of both traces in Figure 9.

This transient effect was only observed for $D_2{}^{18}O$ condensation on bulk ice (B) and single-crystal ice (SC), as vapor phase condensed ice (C) did not support a measurable vapor pressure except at very large injected doses. Therefore, R_{ev} was found to be immeasurably small for condensed ice samples (C). We attribute this lack of evaporation to the porosity of these condensed ice samples. They obviously do not support a $D_2{}^{18}O$ vapor pressure in the aftermath of a $D_2{}^{18}O$ pulse, whereas the bulk ice (B) surfaces let $D_2{}^{18}O$ molecules evaporate back into the vapor phase. Therefore, a large fraction of the condensed water molecules may be retained inside the porous texture of a condensed ice (C) sample,[31,32] unable to desorb on our time scale of several seconds. However, this transient effect of the lack of vapor pressure above a condensed sample (C) is not due to an isotope effect between ordinary ($D_2{}^{16}O$) and heavy ($D_2{}^{18}O$) water. Heras et al.[33] have measured the vapor pressure of $D_2{}^{18}O$ ice at temperatures below 273 K to be lower than the pressure measured above $H_2{}^{16}O$ ice. However, this decrease is insignificant and amounts to a few percent of the vapor pressure.[33] It can therefore not account for the transient decrease of vapor pressure observed on condensed ice (C) in the aftermath of a $D_2{}^{18}O$ pulse.

Another manifestation of this morphological difference between bulk (B) and condensed ice (C) is shown in Figure 10. At 180 K the condensation of a $D_2{}^{18}O$ pulse corresponding to a dose of 5×10^{16} molecules generates a steady-state level on a bulk ice sample (B). However, when a $D_2{}^{18}O$ pulse of identical dose is interacting with a condensed ice sample (C), no steady-state level was observed because the condensed probe molecules are trapped and retained inside the porous texture of the condensed ice (C).

In conclusion, the negative temperature dependence of the net uptake rate constant (k_{eff}) as well as the increased transient vapor pressure of $D_2{}^{18}O$ after pulsed injection suggests the existence of a precursor species whose bonding to the ice surface is weaker than that for H_2O molecules making up the bulk state of ice. This assumption is confirmed by the absence of a steady-state level when using a snow sample (S), which is characterized by a significant internal surface.

Influence of the Type of Ice on the Kinetics. At 140 K, our results clearly indicate that k_{eff} and γ depend on the type of ice sample; values obtained at this temperature on both single crystal ice (SC) and cubic (K) ice strongly differ. At 140 K the highest uptake coefficient for $D_2{}^{18}O$ of $\gamma = 0.8$ was observed for cubic ice samples (K), whereas it decreased to $\gamma = 0.15$ for uptake on single-crystal ice (SC) at the same temperature.

Experiments performed at 180 K on bulk ice (B) or single-crystal ice (SC) confirm this result. The surface of hexagonal single-crystal ice (SC) is characterized by lower densities of surface defects because of the slow cooling conditions. Rapid cooling of deionized liquid water resulting in bulk ice (B) leads to formation of stress cracks during crystal growth as we have observed from photographic pictures where the formation and propagation of cracks become apparent. The surface of a bulk ice (B) sample may therefore be more disordered than the surface of single-crystal ice (SC). We expected therefore that the kinetics of condensation of water on ice strongly depended on the density of surface defects. When the concentration of defects is important, the condensation is apparently faster because these defect sites strongly interact with the gas phase. Thus, k_{eff} measured on single-crystal ice (SC) at 180 K is a factor of 2 lower than that on bulk ice (B).

To test whether the surface properties of ice affected the uptake kinetics, we have compared values of k_{eff} measured at 140 K on a condensed cubic ice sample (K) that was subsequently annealed at different temperatures. The results are shown in Figure 4. The value of k_{eff}, measured at 140 K, decreases by a factor of 2 when the condensed cubic ice sample (K) is annealed at 210 K, leading to a k_{eff} value identical to

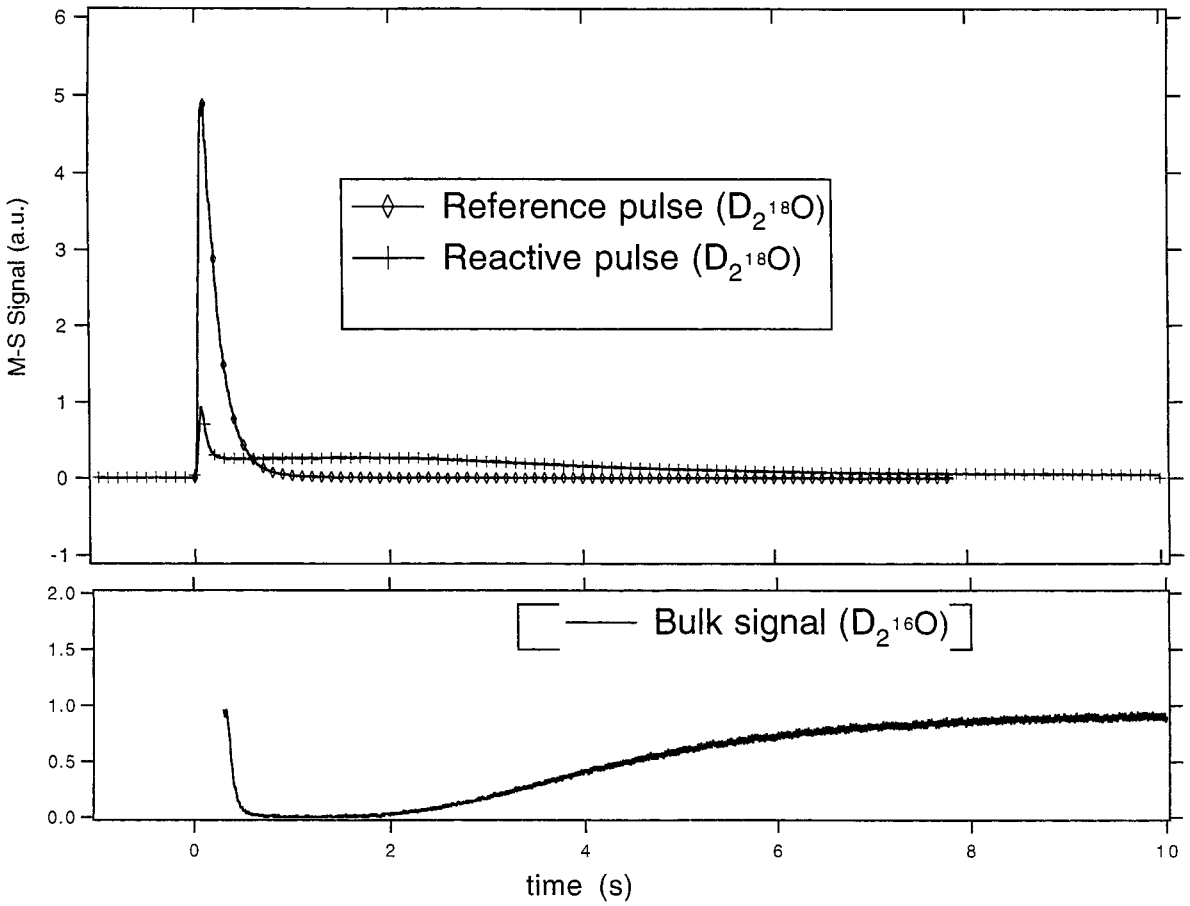

Figure 9. MS signal of reference and reactive pulses at $T = 200$ K of $D_2{}^{18}O$ reacting with a bulk ice (B) sample. The signal corresponding to $D_2{}^{16}O$ represents the effusing beam of water molecules originating from the ice surface and leaving the reactor.

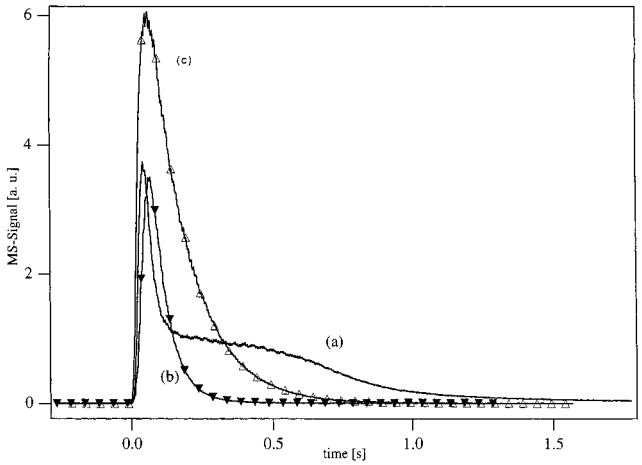

Figure 10. Reactive pulsed valve experiments performed at 190 K: (a) pulse of 5×10^{15} $D_2{}^{18}O$ molecules interacting with a $D_2{}^{16}O$ bulk ice (B) sample and generating a steady-state level; (b) pulse of 5×10^{15} $D_2{}^{18}O$ molecules interacting with a $D_2{}^{16}O$ condensed ice (C) sample, no steady-state level observed; (c) reference pulse of $D_2{}^{18}O$ of 5×10^{15} molecules.

that for a bulk ice sample (B) measured at 140 K. The data presented here indicate that the annealing process of cubic ice changes its condensation kinetics compared to that measured at 140 K. During the formation and slow deposition process of cubic ice (K), the rate of surface reconstruction to a lower potential energy structure is obviously slow in comparaison to the rate of condensation. Therefore, cubic ice may have a more energetic and thus more reactive external surface. In addition, its texture may be porous or microporous, with a highly irregular surface structure and a large fraction of incompletely coordinated surface water molecules.[25,34] Moreover, annealing of cubic ice (K) may be accompanied by the decrease of surface disorder and by the reduction of the number of incompletely coordinated surface water molecules. At the annealing temperature of 180 K, a transition of the ice structure from cubic to hexagonal is expected.[23,24,31,32,35] Many groups have shown that an ice sample obtained by vapor condensation that is annealed to a temperature exceeding 200 K undergoes changes in its internal surface area. They suggested that this reduction of the internal surface was caused by closure of pores upon annealing and sintering. Thus, we propose that these structural changes are accompanied by the disappearance of energetic surface sites allowing efficient condensation and are in turn characterized by high values of k_{eff} and thus of γ. Our experiments thus suggest that both the method of preparation and the thermal history of the sample influence its kinetic properties, which are strongly affected by the morphology and the microstructure of the sample.

On the basis of the present results, we suggest that the different values of γ reported in the literature may partly be reconciled if we assume that uptake experiments were taking place on samples generated by different methods of preparation and on samples of different thermal history. We are thus proposing an explanation for the large spread of uptake coefficients that were measured in previous studies and which were ranging from $\gamma = 0.03$ to 1.0 (Table 6). Figure 11 displays the values of γ obtained by Isono,[36] which agree with our results measured on bulk ice samples (B). Authors[10,37] who measured high values of γ (above 0.6) have performed their experiments on ice prepared by vapor condensation at low temperatures. These previous studies seem to be roughly consistent with our

TABLE 6: Selected Values of H_2O Uptake Coefficients on Ice

γ	temperature range (K)	method	reference
1.00	213−233	gravimetric	Kramers and Stremerding, 1953[9]
0.83	133−158	gravimetric	Koros et al., 1962[10]
1.00	150	IR absorption	Tolbert and Middlebrook, 1990[37]
1.00	145	optical interference technique	Brown et al., 1996[12]
0.98	293	vapor flow loss	Leu, 1988[14]
0.05	285	liquid evaporation	Delaney et al., 1964[42]
0.05−0.35	165−220	ice crystal radial growth	Isono, 1968[36]
0.026	295−298	droplet radial growth	Sinarwalla et al., 1975[43]

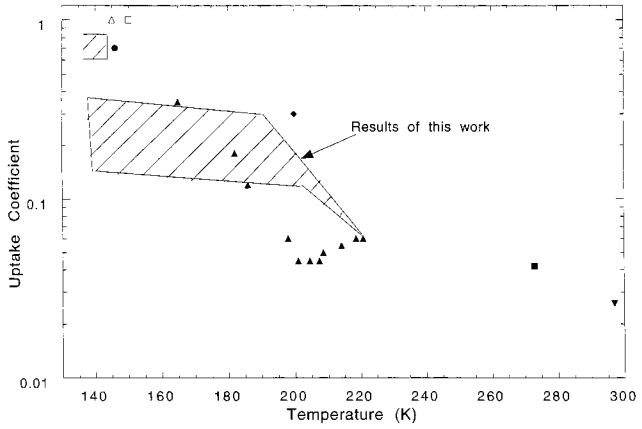

Figure 11. Comparison of $D_2{}^{18}O$ uptake coefficients measured in this work (hatched area) with literature values: (■) Tolbert and Middlebrook (1990);[37] (△) Brown et al. (1996);[12] (●) Koros et al. (1962);[10] (▲) Isono (1968);[36] (◆) Leu (1988);[14] (■) Delaney et al. (1964);[42] (▼) Sinarwalla et al. (1975).[43]

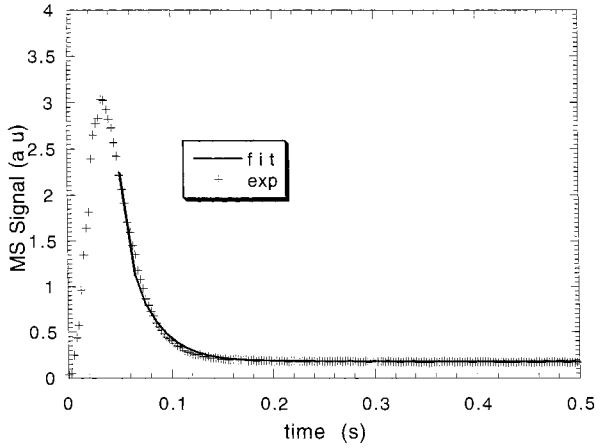

Figure 12. Display of a MS signal of a typical pulsed experiment at 140 K where a dose of 10^{16} $D_2{}^{18}O$ molecules was injected on a condensed ice sample together with the model fit.

SCHEME 2

$$SS + H_2O \underset{k_2}{\overset{k_1}{\rightleftharpoons}} H_2O_{(ads)} \underset{k_4}{\overset{k_3}{\rightleftharpoons}} SS + H_2O_{(bulk)}$$

results. However, a systematic comparison with our results is not possible because they did not describe the details of their ice sample preparation.

Model Calculation. The negative temperature dependence of the net $D_2{}^{18}O$ uptake leads us to propose a complex mechanism[29,30] in order to interpret the condensation of water molecules on ice. This mechanism, which had been proposed by George and co-workers[11] but was later dropped because of new experimental results,[12] involved the formation of one precursor species onto the surface of ice in what was called precursor-mediated adsorption of H_2O on ice.

We similarly interpret our experimental results by using a simple kinetic model in terms of elementary gas and surface processes. Both the negative temperature dependence and the first-order rate are consistent with a precursor mediated mechanism. This mechanism, in which $H_2O_{(ads)}$ assumes the role of precursor, has been described by Scheme 2.

As briefly mentioned above, condensation occurs when a gas-phase molecule $H_2O_{(gas)}$ is trapped by the ice surface on a condensation site SS. This condensation, characterized by the adsorption rate constant k_1 results in the formation of a precursor species $H_2O_{(ads)}$, which consists of water molecules more weakly bound to the surface than $H_2O_{(bulk)}$ making up bulk ice. Subsequently, the precursor species may desorb into the gas phase in a first-order process k_2 or may rearrange to bulk ice to become a thermodynamically stable $H_2O_{(bulk)}$ within the ice in a first-order process k_3.

The above mechanism is given by four rate constants (k_1−k_4), each with a potential positive activation energy, and by three species ($H_2O_{(gas)}$, $H_2O_{(ads)}$, and $H_2O_{(bulk)}$). $H_2O_{(gas)}$ is experimentally observable, whereas $H_2O_{(ads)}$ is not and may never exceed the number of geometric surface sites S_0, which corresponds to the number of molecules making up one formal monolayer. The free surface sites SS obey the mass balance relation $S_0 = SS + H_2O_{(ads)}$.

The goal of this part of our work is to find a set of four rate constants that give the best fit to the measured time-dependent MS signal of $H_2O_{(gas)}$ in each experiment. Assuming $S_0 = 10^{15}$ molecule cm^{-2} and using the injected dose as experimental input data, we are able to adjust the four fit parameters k_1, k_2, k_3, and k_4 in order to find an overall best fit to k_{eff}, which generally resulted in excellent agreement between k_{eff} calculated and observed (Figure 12). The modeling has been extended to include several types of ice samples spanning the temperature range 140−200 K (Figure 6). Table 7 shows representative results of fitted model rate constants at different temperatures for three different types of ice.

Figure 13 displays the best fit of the calculated values of k_{eff} to the experimental data represented as symbols as a function of temperature obtained for each type of ice sample. The results from Table 7 show that the variation of k_{eff} observed for the different types of ice samples is mainly due to a change in the rate constant k_1, which, however, is temperature independent. The other kinetic parameters for desorption (k_2, k_4) and for rearrangement and thus the incorporation of the precursor state into bulk ice (k_3) are less dependent on the type of ice investigated but depend on the temperature. This indicates that the rate of condensation is strongly controlled by the kinetics of adsorption of H_2O on surface sites of ice, SS, thus leading to $H_2O_{(ads)}$ in a kinetic process without an energy barrier.

Table 7 also presents the activation energies for the rate constants (k_1, k_2, k_3, k_4) found by fitting k_{eff}. All the constants have positive activation energies larger than or equal to zero. In particular, we find zero activation energy for k_1, as expected

TABLE 7: Temperature Dependence of the Model Rate Constants (see Scheme 2) in the System $D_2{}^{18}O$ Vapor/ $D_2{}^{16}O$ Ice for Three Temperatures

	single-crystal ice (SC)				condensed ice (C)				bulk ice (B)			
T(K)	k_1[b]	k_2[c]	k_3[c]	k_4[b]	k_1[b]	k_2[c]	k_3[c]	k_4[b]	k_1[b]	k_2[c]	k_3[c]	k_4[b]
140	19	0.5	153	0.005	26	0.6	120	0.005	38	0.3	80	0.02
170	19	5	230	5	26	6.0	180	0.700	38	2.5	130	2.5
200	19	29	310	29.0	26	35.0	243	27	38	25	160	54
E_i (kcal/mol)	0	4.0	0.6	7.4	0	3.8	0.67	8	0	3.9	0.64	8.2
ΔH_{sub}[a] (kcal/mol)		10.8				11.1				11.5		

[a] $\Delta H_{sub} = E_1 - E_2 + E_3 - E_4$. [b] k is expressed in molecule^{-1} s^{-1}. The rate constants take into account the surface-to-volume ratio of the flow reactor used in the present work (Table 1, ω^1). [c] k is expressed in s^{-1}.

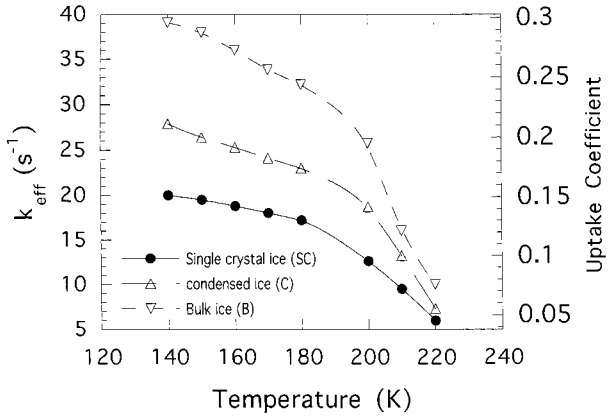

Figure 13. Comparison of calculated k_{eff} obtained from the precursor-mediated condensation model (lines) with typical values of the uptake coefficient of $D_2{}^{18}O$ on different ice surfaces (representative data are taken from Figure 2).

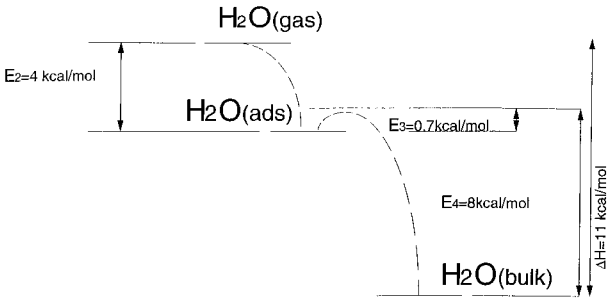

Figure 14. Reaction enthalpy and activation energies for the condensation of water vapor on ice according to the mechanism presented in Scheme 2.

for an elementary adsorption process. The activation energies for evaporation, k_2 and k_4, are positive with values of 4 and 8 kcal/mol, respectively. The model thus predicts a heat of sublimation ΔH_{sub} of ice of approximately 11.4 ± 0.5 kcal/mol at 200 K. When the value is corrected to 300 K using published C_p values, we obtain $\Delta H_{sub} = 11.5 \pm 0.5$ kcal/mol, which is identical to the value found experimentally within the error limits and consistent with the thermodynamic value of H_2O sublimation.

Figure 14 shows a reaction enthalpy plot derived from the activation energies of the modeled rate constants. The activation energies clearly show the existence of two stable thermodynamic states of water in the condensed phase within the H_2O/ice system. The first corresponds to the adsorption of gaseous H_2O onto ice, resulting in a precursor state with a relative stability of 4 kcal/mol with respect to $H_2O_{(gas)}$. The absence of activated adsorption ($E_1 = 0$ kcal/mol) as well as the value of $\Delta E = E_1 - E_2$ points to a hydrogen-bonded state of H_2O on the surface of ice. In agreement with the literature, we may assume that most of the H_2O surface species making up the condensation sites SS are bound to the ice surface by three hydrogen bonds. In comparison, $H_2O_{(bulk)}$ is bound by four hydrogen bonds within a stable ice crystal.[34] At this point, we refrain from assigning a specific bonding situation of $H_2O_{(ads)}$ in terms of the number of hydrogen bonds. We stress that the properties of $H_2O_{(ads)}$ have been derived owing to its kinetic behavior, and it suffices to state that it is a species more loosely bound than $H_2O_{(bulk)}$. The formation of a precursor species has already been proposed by George and co-workers[11] and Davy and Somorjai[38] who assumed that this species consisted of water molecules attached to the surface by one or two hydrogen bonds.

In addition, the process of incorporation of the precursor species into bulk ice involves the small barrier E_3 of 0.7 kcal/mol. The enthalpy difference between the precursor $H_2O_{(ads)}$ and the bulk species $H_2O_{(bulk)}$ suggests that H_2O is first weakly bound to the surface of ice by 4 kcal/mol upon adsorption. This result confirms that surface defects may significantly affect the overall uptake rate constant k_{eff} displayed in Table 7 through the elementary rate constant for initial adsorption k_1. The simulation confirms that the activation energy for evaporation (Table 5) is approximately 8 kcal/mol for the high-temperature range of our experiments, where the rate of evaporation is controlled by process k_4, whereas it is controlled by both k_4 and k_2 in the low-temperature range. This means that the desorption of $H_2O_{(ads)}$ is only limiting at low temperatures.

The present mechanism illustrates one possibility of how gas-phase H_2O molecules are incorporated into bulk ice. The model we have described may be regarded as a result of a sequence of steps associated with definite activation energies corresponding to distinct physical processes. It shows that the kinetics of condensation is strongly controlled by the kinetics of the first step corresponding to the adsorption onto specific reaction sites of ice, which may change from one type of ice to another. These results support the possible influence of surface defects on the overall rate constant k_{eff}; surface defects such as steps, cracks, or dangling OH bonds may constitue favorable sites of adsorption onto an ice surface and consequently more efficient kinetics of adsorption of H_2O vapor. This assumption has already been made previously for the case of nonpolar adsorption of molecules such as CF_4 or CH_4 on ice.[39,40] The rearrangement process k_3 may be understood by considering that $H_2O_{(bulk)}$ is held in place by four hydrogen bonds, whereas molecules on the surface, such as $H_2O_{(ads)}$, are bound by a lower number of hydrogen bonds.[41]

Conclusion and Atmospheric Implications

Pulsed valve experiments were used to measure the condensation coefficients for $D_2{}^{18}O$ on ice surfaces for temperatures in the range 140−220 K. The uptake coefficient γ was observed to decrease with temperature and varied between 0.8 and 0.06 depending on the type of ice sample. This decrease of γ with increasing ice temperature is consistent with a precursor-

mediated condensation model. The value of γ is independent of the dose, corresponding to a first-order process. Vapor pressure measurements support the formation of a precursor species of higher transient vapor pressure. This identifies the precursor as a H_2O molecule that is weakly bound to the ice surface when compared to stable crystalline H_2O constituting the ice matrix. The rate of evaporation F_{ev} reveals the surface to be very dynamic; at 200 K about 70 monolayers evaporate and condense per second at equilibrium.

The data obtained using different types of ice samples clearly exhibit a net dependence of k_{eff} on the ice sample preparation method. We propose that these differences between samples are due to the presence of energetic surface imperfections and/or active adsorption sites that interact more efficiently with gaseous H_2O compared to the majority of surface sites. We also observed a pronounced effect of annealing of the ice sample on k_{eff} and reached the conclusion that it reduced the density of defects or imperfections responsible for the interaction of H_2O gas with ice.

The details of the growth of ice crystals is one of the important questions in cloud physics, glaciology, and crystal growth. It is well-known that the change in morphology of ice crystals growing in air also depends on the mode of formation and on their history. We have suggested that the kinetics of the growth rate of ice crystals depend on their surface microstructure. Thus, to extrapolate laboratory results to atmospheric conditions, the particular ice phase in the atmosphere has to be known before choosing the appropriate kinetic parameters for heterogeneous interaction. This study demonstrated that the thermal history of an ice crystal will affect its surface properties. Thus, we suggest that the mode of formation of ice in the atmosphere may also determine in part its surface properties. For this reason, snow or PSC particles essentially formed by slow gas-phase condensation may have different surface properties than particles formed by rapid freezing of liquid droplets or by riming. Thus, we may suggest that the large value of k_{eff} measured for cubic ice samples (K) in this study may be applicable to atmospheric ice crystals that have been formed for instance in mountain lee waves. Future experiments with the goal to simulate the behavior of atmospheric ice should include the measurement of the concentration of impurities in the ice sample as a possible additional parameter controlling the uptake kinetics of water.

Acknowledgment. The authors acknowledge the generous financial support of the Fonds National Suisse (FNRS). We would like to thank Dr. L. Gutzwiller for the use of his previous experimental results. We also would like to express our gratitude to Professor H.-R. Gäggeler of the University of Bern who provided us with a sample of pure $D_2{}^{18}O$.

References and Notes

(1) Hobbs, P. V. *Ice Physics;* Clarendon Press: Oxford, 1974.
(2) Marti, J.; Mauersberger, K. *Geophys. Res. Lett.* **1993**, *20*, 359.
(3) Bergeron, T. *On the Physics of Clouds and Precipitation;* IASH 5th Assembly IUGG: Lisbon, 1939 156.
(4) Ono, A. *J. Atmos. Sci.* **1969**, *26*, 138.
(5) Pruppacher, H. R. *Microphysics of Clouds and Precipitation*; D. Reidel Pub. Co.: Dordrecht, Holland, 1978.
(6) Chodes, N.; Warner, J.; Gagin, A. *J. Atmos. Sci.* **1974**, *31*, 135.
(7) Toon, O. B.; Turco, R. P.; Jordan, J.; Goodman, J.; Ferry, G. *J. Geophys. Res.* **1989**, *94*, 359.
(8) Turco, R. P. *Atmospheric effects of stratospheric aircraft: a first Program Report*; NASA Ref. Publ. **1992**, *63*, 1272.
(9) Kramers, H.; Stremerding, S. *Appl. Sci. Res. A.* **1953**, *3*, 73.
(10) Koros, R. M.; Deckers, J. M.; Andres, R. P.; Boudart, M. *Chem. Eng. Sci.* **1962**, *18*, 941.
(11) Haynes, D. R.; Tro, N. J.; George, S. M. *J. Phys. Chem.* **1992**, *96*, 8502.
(12) Brown, D. E.; George, S. M.; Huang, C.; Wong, E. K. L.; Rider, K.; Smith, R. S.; Kay, B. *J. Phys. Chem.* **1996**, *100*, 4988.
(13) Bonacci, J. C.; Meyers, A.; Nongbri, G.; Eagleton, L. C. *Chem. Eng. Sci.* **1976,** 31, 609.
(14) Leu, M. T. *Geophys. Res. Lett.* **1988**, *15*, 17.
(15) Alty, T. *Proc. R. Soc. London A* **1931,** *131*, 554.
(16) Levine, N. E. *J. Geophys. Res.* **1973,** *78*, 6266.
(17) Warner, J. *J. Atmos. Sci.* **1969**, *26*, 1272.
(18) Pound, G. M. *J. Phys. Chem. Ref. Data* **1972**, *1*, 135.
(19) Fenter, F. F.; Caloz, F.; Rossi, M. J. *J. Phys. Chem.* **1994**, *98*, 9801.
(20) Fenter, F. F.; Caloz, F.; Rossi, M. J. *J. Phys. Chem*. **1996**, *100*, 1008.
(21) Caloz, F.; Fenter, F.; Tabor, K. D.; Rossi, M. J. *Rev. Sci. Instrum*. **1997**, *68*, 3172. Fenter, F. F.; Caloz, F.; Rossi, M. J. *Rev. Sci. Instrum*. **1997**, *68*, 3180.
(22) Kumai, M. *J. Glaciology* **1968**, *49*, 95.
(23) Defrain, A.; Linh, N. T., *C. R. Hebd. Sceances Acad. Sci.* **1966**, *263*, 1336.
(24) Shalcross, F. V.; Carpenter, G. B., *J. Chem. Phys.* **1957**, *26*, 782.
(25) Westley, M. S.; Baratta, G. A.; Baragiola, R. A. *J. Chem. Phys* **1998**, *108*, 3321.
(26) Gonda, T. J. *Meteorol. Japan* **1976**, *54*, 233.
(27) Gonda, T. J. *Cryst. Growth* **1980**, *49*, 173.
(28) Jancso, G.; Pupezin, J.; Van Hook, W. A. *J. Chem. Phys.* **1970,** *710*, 2984.
(29) Gupta, P.; Mak, C. H.; Coon, P. A.; George, S. M. *Phys. Rev. B* **1990**, *93*, 2827.
(30) Gupta, P.; Coon, P. A.; Koehler, B. G.; George, S. M. *J. Chem. Phys.* **1990**, *93*, 2827.
(31) Keyser, L. F.; Leu, M. T. *J. Colloid Interf*ace *Sci.* **1993**, *155*, 137.
(32) Keyser, L. F.; Leu, M. T. *J. Phys. Chem. B* **1997**, 101.
(33) Heras, J. M. *Chem. Scr.* **1983**, *23*, 244.
(34) Devlin, J. P.; Buch, V. *J. Phys. Chem.* **1995**, *99*, 16535.
(35) Blackman, M.; Lisgarten, N. D. *Proc. R. Soc.* **1957**, *A239*, 93.
(36) Isono, K. Formation and Growth of Ice Crystals at low Pressures. *Proceeding of the International Conference on Cloud Physics, Toronto, Canada*, 1968, 270.
(37) Tolbert, M.; Middlebrook, A. M. *J. Geophys. Res.* **1990**, *95*, 22423.
(38) Davy, V.; Somorjai, L. *J. Phys. Chem*. **1971**, *55*, 3624.
(39) Buch, V.; Deltzeit, L.; Blackledge, C.; Devlin, J. P. *J. Phys. Chem.* **1996**, *100*, 3732.
(40) Chaix, L.; Ocampo, J.; Dominé, F. *C. R. Acad. Sci. II* **1996**, *322*, 609.
(41) Murphy, E. J. *J. Chem Phys.* **1953**, *21*, 1831.
(42) Delaney, L. J.; Houston, R. W.; Eagleton, L. C. *Chem. Eng. Sci.* **1964**, *19*, 105.
(43) Sinarwalla, A. M.; Alofs, D. J.; Carstens, D. J. *J. Atmos. Sci*. **1975**, *32*, 592.